ISSN 0248451X

CENTRE NATIONAL DE LA RECHERCHE SCIENTIFIQUE

SCIENCES POUR L'INGENIEUR

LABORATOIRE D'AEROTHERMIQUE

1C av. de la recherche scientifique, 45071 Orléans Cedex 2
Tél.: +33 (0)2 38 25 03 10 Fax : +33 (0)2 38 25 03 17
e-mail: aero@cnrs-orleans.fr
http://www.cnrs-orleans.fr/~webaero

R 99-2

Numerical computation of shock wave configurations in underexpanded jets

Calcul numérique de configurations d'ondes de choc dans des jets sous-détendus

I.A. Graur, T.G. Elizarova, J.C. Lengrand

Rapport de laboratoire

Juillet 1999

Laboratoire d'Aérothermique : Unité Propre de Recherche du CNRS (UPR9020)
associée par conventions à l'Université d'Orléans et à l'Université Pierre et Marie Curie (Paris 6) et
membre de la Fédération de Recherche FR776 *Energétique, Propulsion, Espace, Environnement*

UNIVERSITE D'ORLEANS

UNIVERSITE PIERRE ET MARIE CURIE

Résumé en français

Problème

Il est bien connu (Abramovich, 1991) qu'un jet sous-détendu axisymétrique présente un **choc en tonneau**. En sortant de la tuyère, le gaz se détend dans le domaine limité latéralement par le choc en tonneau. A quelque distance en aval, le choc en tonneau peut se réfléchir sur l'axe de symétrie comme un disque de Mach associé à un choc réfléchi oblique (**réflexion de Mach**). Sur l'axe, l'écoulement subit une transition du supersonique au subsonique à travers le disque de Mach (Fig.1a).

Dans certaines conditions, une réflexion dite **régulière** (ou simple) peut se produire, sans formation de disque de Mach (Courant, 1948) (Shih-i Pai, 1954) (O'Neill, 1989), (Fig.1b). Ces deux configurations sont étudiées dans le présent travail, par une approche numérique.

Dans un but de validation, un travail préliminaire a consisté à calculer un jet dans des conditions qui correspondent à des résultats expérimentaux obtenus dans l'installation à gaz raréfié SR3 du Laboratoire d'Aérothermique du CNRS (Lengrand et al., 1976).

Les calculs ont consisté en la résolution des équations **quasi gazodynamiques** (QGD) dont la forme générale est donnée plus loin (voir, p;ex. Elizarova et al. 1997). L'algorithme utilisé dans ce travail a été implémenté précédemment pour la simulation numérique de différents problèmes de dynamique des gaz, par exemple l'écoulement autour d'un disque perpendiculaire (Elizarova et al., 1997) (Lengrand et al., 1995). On a montré que les résultats obtenus en résolvant les équations QGD coïncidaient avec ceux des équations de Navier-Stokes (NS) à la limite des faibles nombres de Knudsen.

La même famille de méthodes numériques a été utilisée (voir, p.ex. Antonov, 1998) pour calculer d'autres exemples d'écoulements externes.

Dans le présent rapport, trois ensembles de calculs sont décrits et analysés. Dans le premier, on montre la comparaison entre résultats numériques et données expérimentales obtenues dans l'installation à basse densité SR3 et on démontre l'adéquation à la fois du système d'équations et de la procédure numérique pour traiter le problème considéré. L'influence du maillage et de la régularisation artificielle sur la précision de la solution a été examinée comme dans la Ref. Lengrand et al., 1995.

Dans le deuxième ensemble de calculs, la transition entre les réflexions régulière et de Mach est étudiée pour un niveau de raréfaction donné, en considérant comme variable le nombre de Mach en sortie de tuyère.

Le troisième ensemble contribue à définir l'influence du nombre de Knudsen (raréfaction du jet) sur la transition entre réflexions régulière et de Mach, pour un nombre de Mach d'éjection donné.

Résultats

La comparaison des résultats de calcul avec des données expérimentales et des estimations empiriques montre que la présente méthode est un outil adéquat pour prédire les configurations de choc dans le problème du jet sous-détendu.

La transition de la réflexion de Mach à la réflexion régulière a été étudiée en fonction des nombres de Mach et de Knudsen.

Dans un jet d'azote avec un rapport de pression p_∞/p_e = 0.01, la transition entre réflexions de Mach et régulière se produit pour un nombre de Mach d'éjection Ma_e voisin de 2.4-2.5 si le nombre de Knudsen est petit (Kn_e = 3.42 x 10^{-4}). L'augmentation de Ma_e entraîne un allongement de la première cellule de détente.

Pour un jet de gaz monoatomique de type "sphères rigides", avec Ma_e = 1.1 et p_∞/p_e = 0.1, une variation du nombre de Knudsen de 2 x 10^{-4} à 2 x 10^{-2} change modérément la longueur de la première cellule de détente, mais change le type de réflexion de Mach à régulier pour un nombre de Knudsen voisin de 2 x 10^{-3} - 5 x 10^{-3}.s

Numerical computation of shock wave configurations in underexpanded viscous jets

I.A. Graur[1], T.G. Elizarova[1], J.C. Lengrand[2]

[1]Institute of Mathematical Modeling, Russian Academy of Sciences
Moscow, Russia

[2]Laboratoire d'Aérothermique du CNRS, Orléans, France

Contents

1 Introduction **1**

2 Equations and boundary conditions **2**

3 Computational work **5**
3.1 Computational grid 5
3.2 Boundary layer profiles 6
3.3 Mass-flux approximation at the nozzle exit 6

4 Comparison with experiment **7**

5 Regular and Mach reflection **15**

6 Rarefaction effects **18**

7 Conclusion **24**

Abstract

The present work contributes to investigate the conditions of transition between so-called Mach and regular reflection in underexpanded viscous jets in terms of Mach and Knudsen numbers in the nozzle exit section. Computations were carried out based on quasigasdynamic equations, that were validated by comparison with experimental results obtained in the SR3 low-density facility of the laboratoire d'Aérothermique.

1 Introduction

It is well-known (see e.g., [Abramovich (1991)]) that an axisymmetric underexpanded jet features a barrel shock. Exhausting from the nozzle, the gas expands within the domain limited laterally by the barrel shock. At some distance downstream the barrel shock may reflect on the symmetry axis as a Mach disk associated with an oblique reflected shock (Mach reflection). On the axis, the flow undergoes a supersonic to subsonic transition through the Mach disk (Fig.1a).

Under some conditions, a so-called regular (or simple) reflection may occur without the formation of a Mach disk ([Courant (1948)], [Shih-i Pai (1954)], [O'Neill (1989)], Fig.1b). Both these configurations are studied in the present work based on a numerical approach.

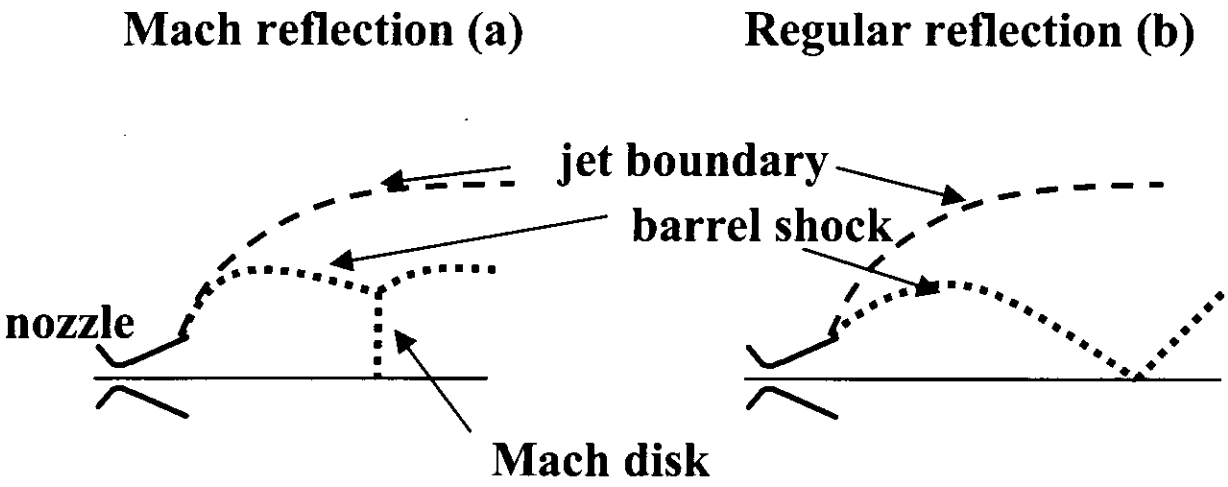

Figure 1: Schematic views of Mach reflection (a) and regular reflection (b) of barrel shock

For validation purpose, a preliminary work consisted in carrying out jet calculations under conditions that correspond to experimental results obtained in the SR3 low-density facility of the laboratoire d'Aérothermique [Lengrand et al. (1976)].

Calculations consisted in solving the quasigasdynamic (QGD) equations whose general form is given hereafter (see, e.g., [Elizarova et al. (1997)]). The computational algorithm used in the present work was implemented earlier for numerical simulations of different gas dynamic problems, e.g., the flow around a perpendicular disk ([Elizarova et al. (1997)], [Lengrand et al. (1995)]). The results obtained by solving QGD equations were shown to coincide with Navier-Stokes results in the limit of vanishing Knudsen numbers.

The same family of numerical methods was used (see, e.g., [Antonov et al. (1998)]) to compute other examples of external flows.

In the present report three sets of computations are described and analysed. In the first one the comparison between numerical results and experimental data obtained in the SR3 low-density facility is shown and demonstrates the adequacy of both the equation system and the associated numerical procedure for treating the problem under consideration. The influence of space grid and artificial regularization on the accuracy of the solutions has been examined as in [Lengrand et al. (1995)].

In the second set of computations the transition between Mach and regular reflections is investigated for a given rarefaction level with the nozzle exit Mach number considered as a variable.

The third set contributes to define the influence of Knudsen number (jet rarefaction) on the transition between Mach and regular reflections in the jet, for a given nozzle exit Mach number.

2 Equations and boundary conditions

QGD equations were obtained by a kinetic approach that consists in integrating the Boltzmann equation multiplied by collisional invariants and using a serial expansion for the distribution function ([Elizarova et al. (1999)]). They were also obtained from a continuum mechanics approach ([Sheretov (1997)]). For stationary flows, the dissipative terms in QGD equations are similar to Navier-Stokes ones (NS), with an additional contribution of order $O(\tau^2)$ or, in a dimensionless form, of order $O(Kn^2)$, where Kn is the Knudsen number.

With usual notations, the general form of QGD system is written as

$$\frac{\partial}{\partial t}\rho + \nabla_i \rho\, u^i - \nabla_i \tau \left(\nabla_j \rho\, u^i u^j + \nabla^i p\right) = 0,$$

$$\frac{\partial}{\partial t}\rho\, u^k + \nabla_i \rho\, u^i u^k + \nabla^k p = \nabla_i\, \tau\, (\nabla_j \rho\, u^i u^j u^k + \nabla^i\, p\, u^k + \nabla^k\, p\, u^i) + \nabla^k\, \tau\, \nabla_i\, p\, u^i,$$

$$\frac{\partial}{\partial t}E + \nabla_i u^i (E+p) = \nabla_i\, \tau\, (\nabla_j (E+2p) u^i u^j + \frac{1}{2}\nabla^i u_k u^k p) +$$
$$\frac{\gamma}{\gamma-1}(\nabla_i\, \tau\, \frac{p}{\rho}\nabla^i\, p + \frac{1}{Pr}\nabla_i\, \tau\, p\, \nabla^i \frac{p}{\rho}),$$

where $E = (\rho u_i^2)/2 + p/(\gamma-1)$, $p = \rho(\mathcal{R}/\mathcal{M})T$, $\tau = \mu/p$, μ is the viscosity coefficient, Pr is the Prandtl number, γ is the specific heat ratio, $\mathcal{M}$ is the molar mass, $\mathcal{R}$ is the universal gas constant.
The axisymmetric form of these equations in (r, z) co-ordinates is

$$\frac{\partial \rho}{\partial t} + \frac{1}{r}\frac{\partial}{\partial r}\left(r\rho u_r\right) + \frac{\partial}{\partial z}(\rho u_z) = \frac{1}{r}\frac{\partial}{\partial r}\left(\tau \frac{\partial}{\partial r} r\rho {u_r}^2\right) + \frac{\partial}{\partial z}\left(\tau \frac{\partial}{\partial z}\rho {u_z}^2\right) +$$
$$\frac{1}{r}\frac{\partial}{\partial r}\left(r\tau\frac{\partial p}{\partial r}\right) + \frac{\partial}{\partial z}\left(\tau\frac{\partial p}{\partial z}\right) + \frac{1}{r}\frac{\partial}{\partial r}\left(r\tau\frac{\partial}{\partial z}\rho u_r u_z\right) + \frac{\partial}{\partial z}\left(\frac{\tau}{r}\frac{\partial}{\partial r} r\rho u_r u_z\right),$$

$$\frac{\partial \rho u_r}{\partial t} + \frac{1}{r}\frac{\partial}{\partial r}\left(r\rho {u_r}^2\right) + \frac{\partial}{\partial z}\left(\rho u_r u_z\right) + \frac{\partial p}{\partial r} = \frac{1}{r}\frac{\partial}{\partial r}\left(\tau\frac{\partial}{\partial r} r\rho {u_r}^3\right) +$$
$$\frac{\partial}{\partial z}\left(\tau\frac{\partial}{\partial z}\rho u_r {u_z}^2\right) + 2\frac{1}{r}\frac{\partial}{\partial r}\left(r\tau\frac{\partial p u_r}{\partial r}\right) - 2p\tau\frac{u_r}{r^2} + \frac{\partial}{\partial r}\left(\frac{\tau}{r}\frac{\partial}{\partial r} r p u_r\right) + \frac{\partial}{\partial z}\left(\tau\frac{\partial p u_r}{\partial z}\right) +$$
$$\frac{1}{r}\frac{\partial}{\partial r}\left(r\tau\frac{\partial}{\partial z}\rho {u_r}^2 u_z\right) + \frac{\partial}{\partial z}\left(\frac{\tau}{r}\frac{\partial}{\partial r} r\rho {u_r}^2 u_z\right) + \frac{\partial}{\partial r}\left(\tau\frac{\partial p u_z}{\partial z}\right) + \frac{\partial}{\partial z}\left(\tau\frac{\partial p u_z}{\partial r}\right),$$

$$\frac{\partial \rho u_z}{\partial t} + \frac{1}{r}\frac{\partial}{\partial r}\left(r\rho u_r u_z\right) + \frac{\partial}{\partial z}\left(\rho {u_z}^2\right) + \frac{\partial p}{\partial z} =$$
$$\frac{1}{r}\frac{\partial}{\partial r}\left(\tau\frac{\partial}{\partial r} r\rho {u_r}^2 u_z\right) + \frac{\partial}{\partial z}\left(\tau\frac{\partial}{\partial z}\rho {u_z}^3\right) + \frac{1}{r}\frac{\partial}{\partial r}\left(r\tau\frac{\partial p u_z}{\partial r}\right) + 3\frac{\partial}{\partial z}\left(\tau\frac{\partial p u_z}{\partial z}\right) +$$
$$\frac{1}{r}\frac{\partial}{\partial r}\left(r\tau\frac{\partial}{\partial z}\rho u_r {u_z}^2\right) + \frac{\partial}{\partial z}\left(\frac{\tau}{r}\frac{\partial}{\partial r} r\rho u_r {u_z}^2\right) + \frac{1}{r}\frac{\partial}{\partial r}\left(r\tau\frac{\partial p u_r}{\partial z}\right) + \frac{\partial}{\partial z}\left(\frac{\tau}{r}\frac{\partial}{\partial r} r p u_r\right),$$

$$\frac{\partial E}{\partial t} + \frac{1}{r}\frac{\partial}{\partial r} r u_r (E+p) + \frac{\partial}{\partial z} u_z (E+p) =$$
$$\frac{1}{r}\frac{\partial}{\partial r}\left(\tau\frac{\partial}{\partial r} r {u_r}^2 (E+2p)\right) + \frac{\partial}{\partial z}\left(\tau\frac{\partial}{\partial z} {u_z}^2 (E+2p)\right) +$$
$$\frac{1}{r}\frac{\partial}{\partial r}\left(r\tau\frac{\partial}{\partial r} p\frac{{u_r}^2}{2}\right) + \frac{\partial}{\partial z}\left(\tau\frac{\partial}{\partial z} p\frac{{u_z}^2}{2}\right) + \frac{1}{r}\frac{\partial}{\partial r}\left(r\tau\frac{\partial}{\partial r} p\frac{{u_z}^2}{2}\right) + \frac{\partial}{\partial z}\left(\tau\frac{\partial}{\partial z}\frac{p {u_r}^2}{2}\right) +$$
$$\frac{\gamma}{\gamma-1}\left(\frac{1}{r}\frac{\partial}{\partial r}\left(\frac{p\tau}{\rho} r\frac{\partial p}{\partial r}\right) + \frac{\partial}{\partial z}\left(\frac{p\tau}{\rho}\frac{\partial p}{\partial z}\right)\right) + \frac{\gamma Pr^{-1}}{\gamma-1}\left(\frac{1}{r}\frac{\partial}{\partial r}\left(p\tau r\frac{\partial}{\partial r}\frac{p}{\rho}\right) + \frac{\partial}{\partial z}\left(p\tau\frac{\partial}{\partial z}\frac{p}{\rho}\right)\right) +$$
$$\frac{1}{r}\frac{\partial}{\partial r}\left(\tau r\frac{\partial}{\partial z} u_r u_z (E+2p)\right) + \frac{\partial}{\partial z}\left(\frac{\tau}{r}\frac{\partial}{\partial r} r u_r u_z (E+2p)\right).$$

The equation of state and the expression of energy close the system.
For the coefficient of viscosity a power-law temperature dependence is taken in the form

$$\mu = \mu_{ref}\left(\frac{T}{T_{ref}}\right)^{\omega},$$

that is compatible with a *Variable Hard Sphere (VHS)* intermolecular potential ([Bird (1998)]).

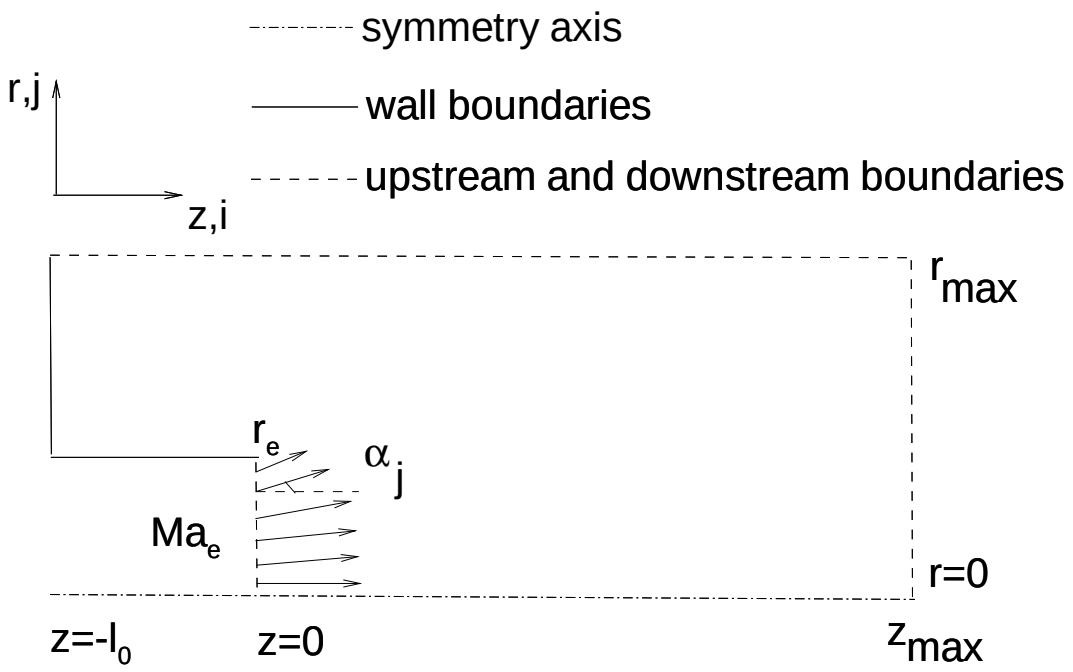

Figure 2: Computational domain.

The subscripts e and ∞ correspond to nozzle exit and background gas, respectively. The Knudsen number is defined as $Kn_e = \lambda_e/(2r_e)$, where r_e is the radius of the nozzle exit.

The computational domain is shown schematically in Fig. 2. The nozzle exit was located at $z = 0$. The left boundary of the computational domain was located at $z = -l_0 = -20\, r_e$. The boundary conditions were as follows

- On the left boundary

  nozzle exit section

  $$\vec{u}(r) = \vec{U}(r), \quad p(r) = p_e, \quad T(r) = T_e(r),$$

  outside the nozzle (on the walls)

  $$u_z = 0, \qquad u_r = 0, \qquad \frac{\partial p}{\partial n} = 0, \qquad \frac{\partial T}{\partial n} = 0,$$

  where n is the direction normal to the wall.

- On the right (downstream) boundary, so-called "soft" conditions were prescribed:

  $$\frac{\partial u_z}{\partial z} = 0, \quad \frac{\partial u_r}{\partial z} = 0, \quad \frac{\partial p}{\partial z} = 0, \quad \frac{\partial T}{\partial z} = 0.$$

- On the upper (lateral) boundary (background gas):

$$\frac{\partial u_z}{\partial r} = 0, \quad u_r = 0, \quad p = p_\infty, \quad T = T_\infty.$$

- On the symmetry axis:

$$\frac{\partial u_z}{\partial r} = 0, \qquad u_r = 0, \qquad \frac{\partial p}{\partial r} = 0, \qquad \frac{\partial T}{\partial r} = 0.$$

For comparison purpose, the extent of the first expansion cell (abscissa of the first shock on the nozzle axis) can be estimated by an expression obtained for a non-viscous non-heat-conducting gas ([Abramovich (1991)])

$$z_{\text{cell}}^{AB} = (2\,r_e) \times 0.896\, Ma_e \sqrt{\gamma\, p_e/p_\infty}. \tag{1}$$

Another expression was proposed ([Ashkenas (1964)]) for jets from sonic orifices

$$z_{\text{cell}}^{AS} = (2\,r_e) \times 0.67 \sqrt{p_0/p_\infty}, \tag{2}$$

where p_0 is the stagnation pressure.
[Lengrand et al. (1982)] propose the expression

$$z_{\text{cell}}^{L} = (2\,r_e) \times F(Ma_e, \alpha_e) \sqrt{p_0/p_\infty}, \tag{3}$$

with

$$F = 0.393 \frac{r_c}{r_e} \left(\frac{\gamma-1}{2}\right)^{-0.6315} \left(\frac{\theta_\infty}{\pi/2}\right)^{-0.96}$$

$$\theta_\infty = \nu(Ma \to \infty) - \nu(Ma_e) + \alpha_e,$$

where $\nu(Ma)$ is the Prandtl-Meyer angle

$$\nu = \sqrt{\frac{\gamma+1}{\gamma-1}} \arctan \sqrt{\frac{\gamma-1}{\gamma+1}(Ma^2-1)} - \arctan\sqrt{Ma^2-1}$$

and α_e is the nozzle half-angle of divergence. The derivation of this estimation is based on the pressure jump across a normal shock. Thus its validity is expected to be limited to configurations with a Mach disk.

3 Computational work

3.1 Computational grid

The computational domain (Fig.2) is covered by a rectangular grid with non uniform space-steps (h^r) along the r-direction and uniform space-steps (h^z) along the z-direction ($h^z = r_e$ or $0.1r_e$). In the nozzle exit section the grid is uniform in the $r-$direction $h^r = h^r_{min} = 0.1r_e$ or $0.04r_e$ (see Table 1). Outside the nozzle, h^r increases by a constant factor k_r ($1 \le k_r \le 1.2$) between adjacent cells, starting from h^r_{min}. The limit r_{max} of the computational domain in the r-direction is taken sufficiently large for the upper boundary to be located entirely in the undisturbed freestream. Other details of the computational algorithm concerning finite-difference approximation and numerical method can be found in [Lengrand et al. (1995)].

3.2 Boundary layer profiles

The velocity and temperature profiles at nozzle exit were introduced as laminar boundary layer profiles taken from [Schlichting (1955)]

$$\frac{U(y)}{u_e} = \left(1.5\frac{y}{\delta} - 0.5\left(\frac{y}{\delta}\right)^3\right),$$
$$\frac{T_e(y)}{T_e} = 1 + \sqrt{Pr}\frac{\gamma-1}{2}Ma_e^2\left(1 - \left(\frac{U(y)}{u_e}\right)^2\right) + \frac{T_w - T_0}{T_e}\left(1 - \frac{U(y)}{u_e}\right), \quad (4)$$

where y is the distance from the wall and T_0 is the stagnation temperature. Outside the boundary layer, flow parameters were taken as uniform.

To take into account the divergence of the flow at nozzle exit, the angle between the velocity vector and the z-axis was varied from zero on the axis to the nozzle half-angle of divergence α_e at the wall. The angle of the velocity vector in cell j was expressed as

$$\alpha_j = \alpha_e\frac{j-1}{n-1},$$

where n is the number of grid points along the nozzle radius. The flow velocity $U(r)$ was decomposed as

$$u_{ze}(r) = U(r)\cos\alpha_j \qquad \text{and} \qquad u_{re}(r) = U(r)\sin\alpha_j,$$

where r varied from 0 to r_e and α_j varied from 0 to α_e. The distance y from the wall was expressed as

$$y = (r_e - r)\cos\alpha_e$$

in the boundary layer profiles (4).

Thus the present calculation accounts approximately for the divergence and the non-uniformity of the flow at nozzle exit.

3.3 Mass-flux approximation at the nozzle exit

In the QGD model the mass-flux along the i-direction is defined as [Sheretov (1997)]

$$J_i = \rho u^i - \tau(\nabla_j \rho u^i u^j + \nabla^i p).$$

In the axisymmetric case ($(r-z)$ coordinates) the mass-flux along the z- direction is equal to

$$J_z = \rho u_z - \tau\frac{\partial}{\partial z}(\rho u_z^2 + p) - \frac{\tau}{r}\frac{\partial}{\partial r}(r\rho u_z u_r). \quad (5)$$

The nozzle exit section (subscript e) is placed between the computational nodes $1,j$ and $2,j$. The flow parameters at the nozzle exit section can be expressed as, e.g. $\rho_{e,j} = 0.5(\rho_{1,j} + \rho_{2,j})$. Taking into account that the flow parameters at the nozzle exit are known as boundary conditions, it is possible to calculate the flow parameter in the first computational node as e.g. $\rho_{1,j} = 2\rho_{e,j} - \rho_{2,j}$. This approach was used to prescribe density, pressure and velocity component u_r. The velocity component u_z was computed based on the value of mass-flux at the nozzle exit. We assume that in each point of the exit section e,j the QGD mass flux (5) is equal to the prescribed local value of ρu_{ze}. The finite-difference approximation of expression (5) is written as

$$J_{e,j} = 0.5((\rho u_z)_{1,j} + (\rho u_z)_{2,j})^k - \frac{\tau_{e,j}}{h^z}\left((\rho u_z^2 + p)_{2,j} - (\rho u_z^2 + p)_{1,j}\right)^k - \frac{1}{h^z}\left(\frac{\tau}{r}\frac{\partial}{\partial r}(r\rho u_z u_r)_{e,j}\right)^{k-1}. \quad (6)$$

The last term in this expression with the derivatives along the boundary is calculated using the values from the previous time step $(k-1)$, where k is time step index. Assuming $J_{e,j} = \rho_{e,j}u_{e,j}$, (6) appears

as a second order equation for $u_{z_{1,j}}$. The solution of this equation gives two values of the velocity $u_{z_{1,j}}$. Choosing the positive value, we have the expression for the velocity component in the form:

$$u_{z_{1,j}} = h^z \left(\sqrt{D} - 0.5\rho_{1,j}\right)/(2\tau_{e,j}\rho_{1,j}), \qquad \text{where}$$

$$D = 0.25\rho_{1,j}^2 + 4\frac{\tau_e}{h^z}\rho_{1,j}\left(\rho_{e,j}u_{e,j} - 0.5(\rho u_z)_{2,j} + \frac{\tau_{e,j}}{h^z}\left((\rho u_z^2 + p)_{2,j} - p_{1,j}\right) + \frac{1}{h^z}\left(\frac{\tau}{r}\frac{\partial}{\partial r}(r\rho u_z u_r)\right)_{e,j}^{k-1}\right).$$

This way of setting boundary conditions ensures both the correct mass-flow and consistency of the computational algorithm.

In fact, in the range of Knudsen numbers considered here, the terms in factor of τ in Eq.5 are negligibly small compared with ρu_z. Thus u_z could have been prescribed in the same way as the other parameters. This was confirmed by nearly identical results obtained for a few calculations that were repeated with u_z prescribed by the simple expression $u_{z,1,j} = 2u_{z,e,j} - u_{z,2,j}$.

4 Comparison with experiment

Computations were carried out for a Nitrogen jet ($\gamma = 1.4$, $\omega = 0.74$, $Pr = 0.736$) and for the following nozzle exit parameters $p_e = 1177\,\text{Pa}$, $T_e = 208\,\text{K}$, $Ma_e = 4.63$, $Kn_e = 6.75 \times 10^{-4}$. The temperature in the background gas was $T_\infty = 290\,\text{K}$. Two values of the pressure in the background gas were considered, namely $p_\infty = 30.66\,\text{Pa}$ and $p_\infty = 0.668\,\text{Pa}$. The nozzle had a conical divergent with a half-angle $\alpha_e = 10°$, and a wall temperature estimated as $T_w = 450\,\text{K}$. The boundary layer thickness at nozzle exit was estimated to be $\delta = 0.239\,r_e$. All these quantities correspond to experimental conditions taken from [Lengrand et al. (1976)] indicated in Table 1 as run V1, along with parameters that characterize the numerical calculation.

run	V1	V2	V3
Ma_e	4.63	$1.1 - 4.22$	1.1
Kn_e	$6.75 \cdot 10^{-4}$	$3.42 \cdot 10^{-4}$	$2.0 \cdot 10^{-2} - 2.0 \cdot 10^{-4}$
p_e/p_∞	$38.3, 1760.5$	100.	$5., 10.$
r_{max}/r_e	30, 100	75	4
h^r_{min}/r_e	0.1	0.1	0.04
h^r_{max}/r_e	2.7	3.6	0.3
h^z/r_e	1.	1.	0.1
α	0.1	$0.005 - 0.1$	$0.02 - 0.04$
β	0.1	0.2	$0. - 0.2$
$(N_z \times N_r)_{grid}$	111×47	201×86	201×45
N_{iter}	$2.9 \cdot 10^5 - 5.1 \cdot 10^6$	$8.7 \cdot 10^5 - 3.3 \cdot 10^6$	$7.0 \cdot 10^4 - 1.7 \cdot 10^5$

Table 1: Characteristic parameters of QGD runs

The conditions $p_e/p_\infty = 38.3$ have been considered first. The nozzle mass-flow is estimated to be $\mathcal{J} = 2.4 \cdot 10^{-4}$ kg/s. According to Eq.5, the mass-flow through the nozzle exit is

$$\mathcal{J} = 2\pi r_e \int_0^{r_e} j_z(r)\, r\, dr = 2.50\,\text{kg/s} \approx 2\pi r_e \int_0^{r_e} \rho(r)\, u_z\,(r)\, r\, dr = 2.49 \cdot 10^{-4} kg/s.$$

The difference with the estimated experimental mass-flow is essentially due to the approximate character of the boundary layer profile used at nozzle exit.

Density iso-lines have been plotted in Fig. 3, isobars in Fig. 4 and iso-Mach lines in Fig. 5. The flow investigated is characterized by a strong non-uniformity. Density and pressure vary by several orders of

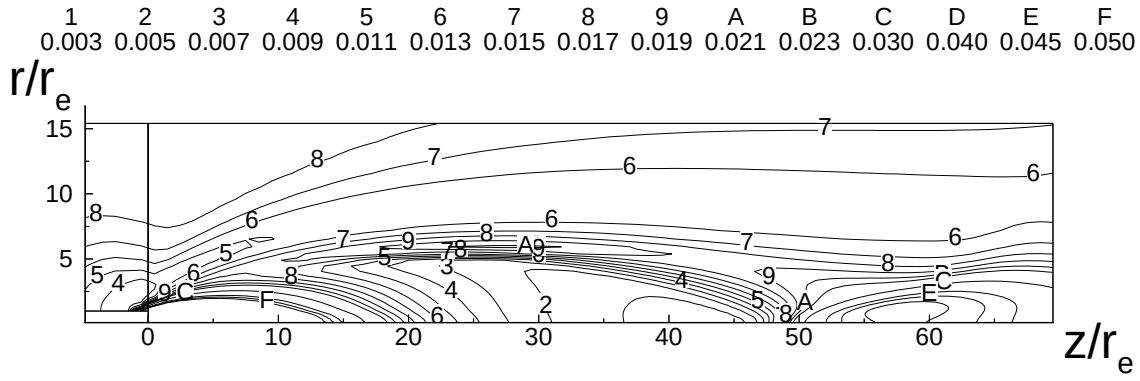

Figure 3: Iso-density lines. $Ma_e = 4.63$, $p_e/p_\infty = 38.3$.

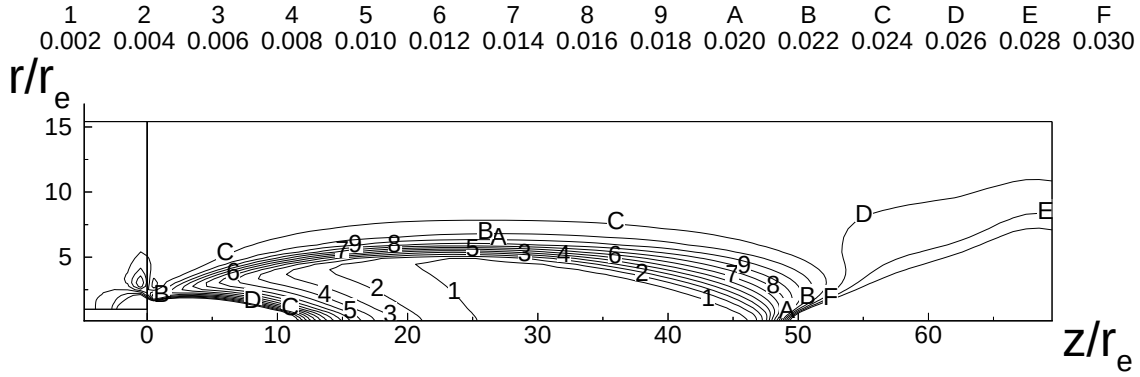

Figure 4: Isobars. $Ma_e = 4.63$, $p_e/p_\infty = 38.3$.

magnitude in both the axial and radial directions. Exhausting from the nozzle, the gas expands and forms a barrel shock. Downstream, the barrel shock reflects on the symmetry axis where the flow undergoes a supersonic to supersonic transition through an oblique shock that decreases the Mach number. In this case regular reflection occurs without the formation of a Mach disk. Near the sharp edge of the nozzle a small vortex forms (not visible in the figures plotted).

The axial density distribution normalized by the stagnation density ($\rho_0 = 1.225\,\mathrm{kg/m^3}$) is plotted in Fig. 6 along with the experimental results [Lengrand et al. (1976)] that were obtained by the electron beam fluorescence technique. For comparison the calculated data obtained with $\omega = 1$ are also presented and can hardly be distinguished from those obtained with $\omega = 0.74$. Refining the grid in the z-direction shifts the results somewhat closer to the experimental ones. The calculated shock position corresponds to the experimental one. If the shock position is taken as the location where the density gradient is a maximum, both the calculation and the experiment locate the shock at $z_{\mathrm{cell}}/r_e = 51$ on the jet axis. Using the empirical relation (1) returns the location $z^{AB}_{\mathrm{cell}}/r_e = 60.7$. Relation (2) returns the location $z^{AS}_{\mathrm{cell}}/r_e = 153.0$, confirming its inadequacy for jets from supersonic nozzles.
In contrast with Eqs.1 and 2, relation 3 takes into account the divergence angle $\alpha_e = 10\,$degrees and

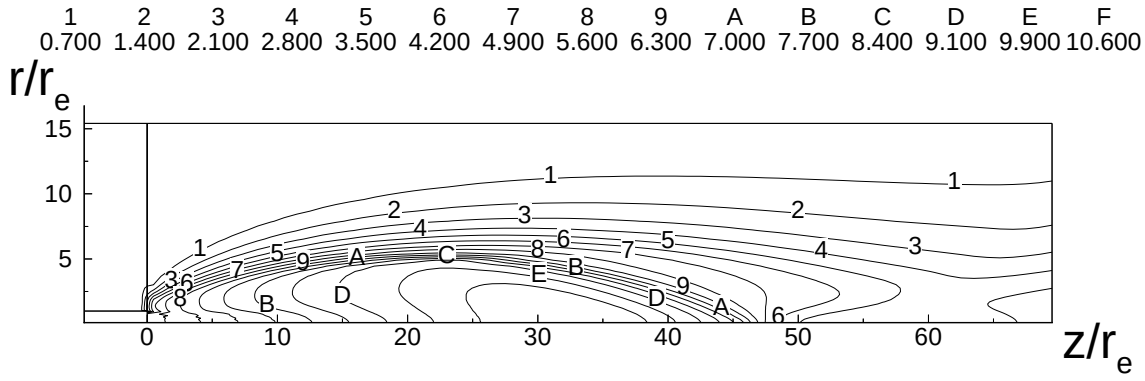

Figure 5: Iso-Mach lines. $Ma_e = 4.63$, $p_e/p_\infty = 38.3$.

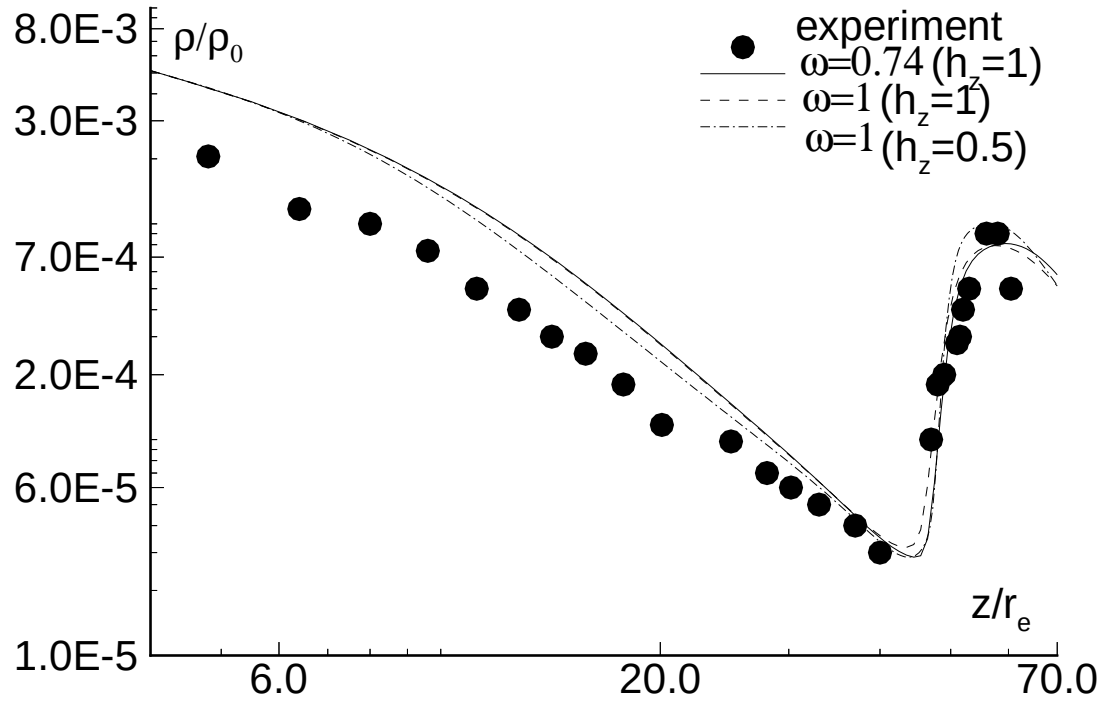

Figure 6: Comparison with experiment. Density distribution along jet axis in logarithmic co-ordinates ($Ma_e = 4.63$, $p_e/p_\infty = 38.3$).

returns $z^L_{\rm cell}/r_e = 76.1$, confirming its inadequacy for jets with regular shock reflection.

The axial density distribution agrees reasonably well with the experimental one.

The jet with pressure ratio $p_e/p_\infty = 1760.5$ features also a barrel shock. According to Eq.1, the barrel

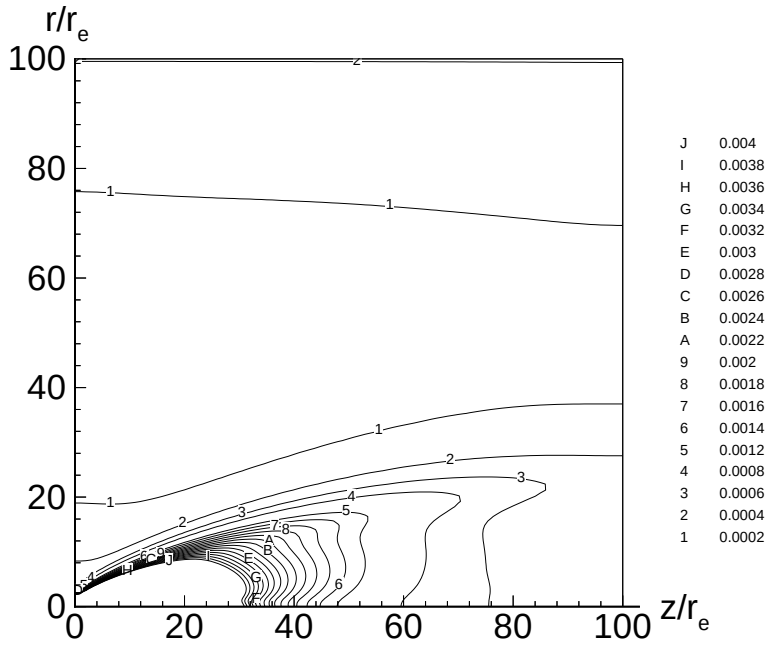

Figure 7: Iso-density lines. $Ma_e = 4.63$, $p_e/p_\infty = 1760.5$.

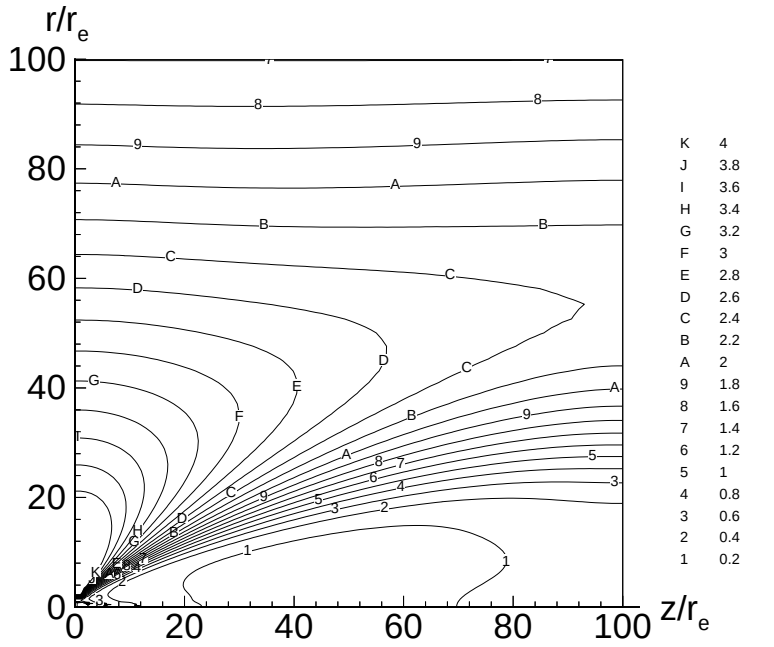

Figure 8: Isotherms. $Ma_e = 4.63$, $p_e/p_\infty = 1760.5$.

shock reflects on the symmetry axis at $z_{cell}/r_e \approx 206.0$, while the maximum dimension of the computational domain in the z- direction is $z_{max}/r_e = 100$. Thus the reflection of the barrel shock takes place outside the computational domain. Density, temperature and Mach number iso- lines have been plotted

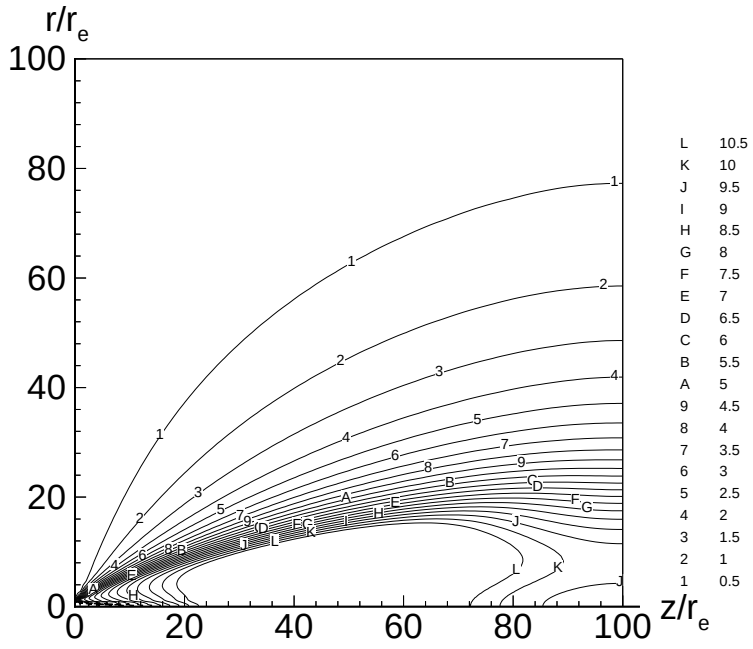

Figure 9: Iso-Mach lines. $Ma_e = 4.63$, $p_e/p_\infty = 1760.5$.

in Fig. 7, 8 and 9, respectively.

The axial density distribution is plotted in Fig 10 along with the experimental one [Lengrand et al. (1976)]. For this case, the (rotational) temperature distribution had been measured experimentally. Axial temperature distributions obtained from the calculation and from the experiment are plotted in Fig.11. While axial density profiles exhibit a satisfactory agreement, the calculated temperature raises unexpectedly at abscissas larger than $(30 - 40)r_e$. A discrepancy between calculated and experimental off-axis densities is also visible on transverse density profiles for abscissas larger than $(30 - 40)r_e$ (Figs.12-17). Note that the abscissa used in Figs.12-17 is $\arctan(\theta)$ where θ is the polar angle in the jet flowfield. Thus under the hypothesis of a source flow expansion, the density profiles in these figures are expected to be identical in the central part of the jet, unaffected by the external pressure.

The reason for this behavior is yet unclear. However, this phenomenon takes place in a region characterized by thermodynamic nonequilibrium, where the validity of a continuum approach is questionable. This is made visible by computing Bird's rarefaction parameter [Bird (1998)]

$$\mathcal{P} = Ma\sqrt{\frac{\gamma\pi}{8}}\frac{\lambda}{\rho}\frac{\partial\rho}{\partial s}, \tag{7}$$

where s is a distance along a streamline. Translation nonequilibrium is known to occurs when $\mathcal{P}$ exceeds 0.02, which can be considered as the limit of continuum approaches. The axial distribution of $\mathcal{P}$ for the present conditions was calculated and plotted in Fig.11. It is clear that the region beyond $z/r_e = 15$ is not in equilibrium ($\mathcal{P} > 0.02$).

The comparison of computed jet flowfields with the corresponding experimental ones gives confidence in the ability of QGD equations and associated numerical techniques to solve jet problems in the parameter range where continuum equations are expected to be valid.

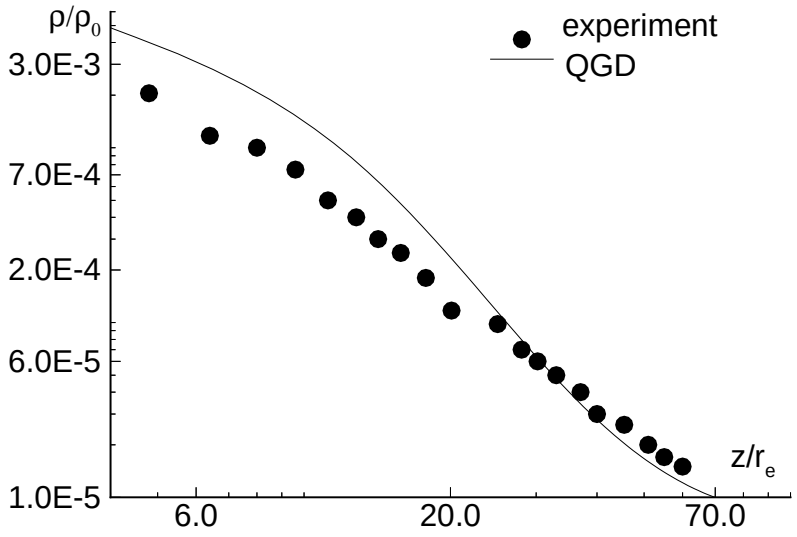

Figure 10: Comparison with experiment. Density distribution in logarithmic scales along jet axis ($Ma_e = 4.63$, $p_e/p_\infty = 1760.5$).

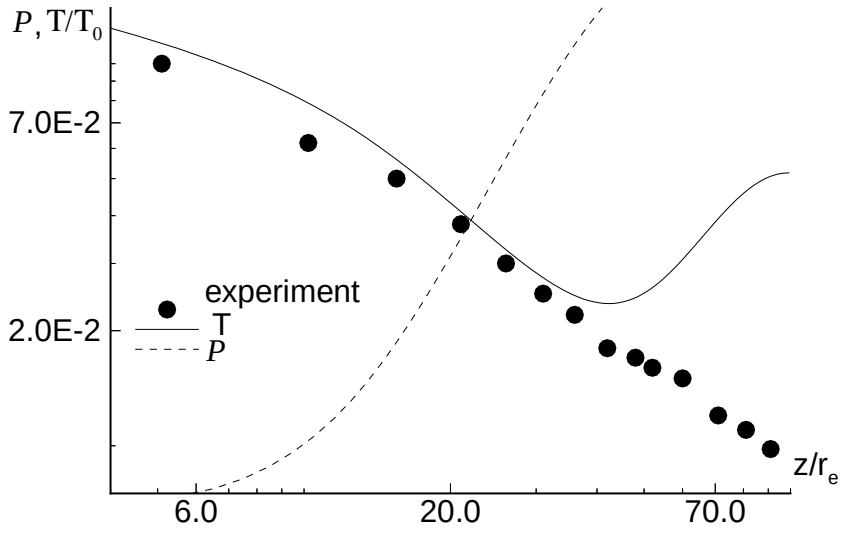

Figure 11: Comparison with experiment. Distributions of temperature and Bird's rarefaction parameter $\mathcal{P}$ along jet axis (logarithmic scales, $Ma_e = 4.63$, $p_e/p_\infty = 1760.5$).

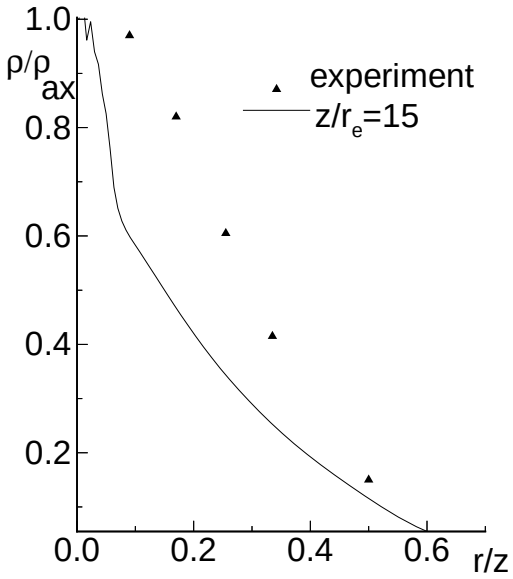

Figure 12: Transverse density profiles at $z = 15\,r_e$, ($Ma_e = 4.63$, $p_e/p_\infty = 1760.5$).

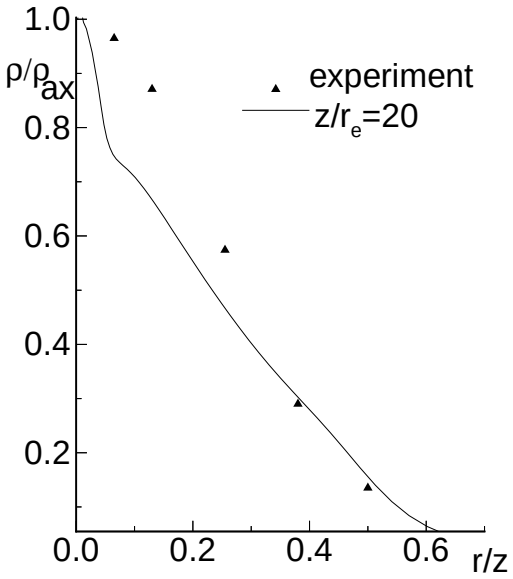

Figure 13: Transverse density profiles at $z = 20\,r_e$, ($Ma_e = 4.63$, $p_e/p_\infty = 1760.5$).

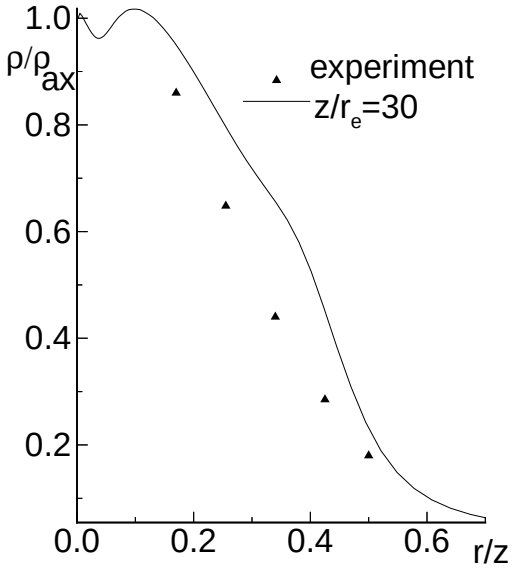

Figure 14: Transverse density profiles at $z = 30\,r_e$, ($Ma_e = 4.63$, $p_e/p_\infty = 1760.5$).

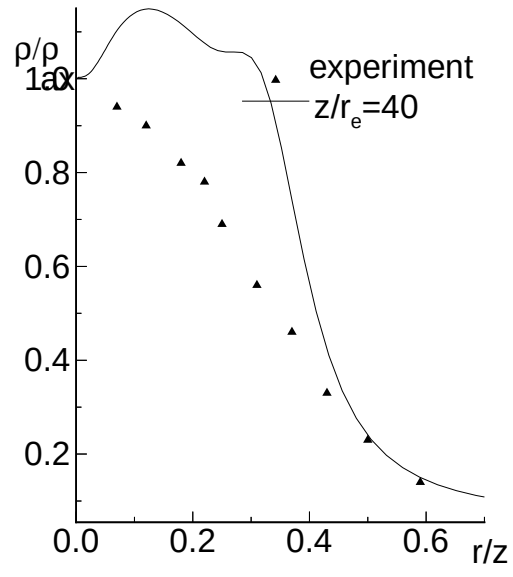

Figure 15: Transverse density profiles at $z = 40\,r_e$, ($Ma_e = 4.63$, $p_e/p_\infty = 1760.5$).

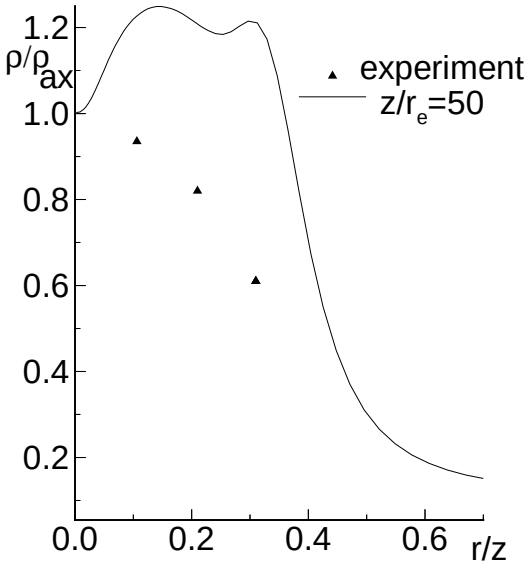

Figure 16: Transverse density profiles at $z = 50\,r_e$, ($Ma_e = 4.63$, $p_e/p_\infty = 1760.5$).

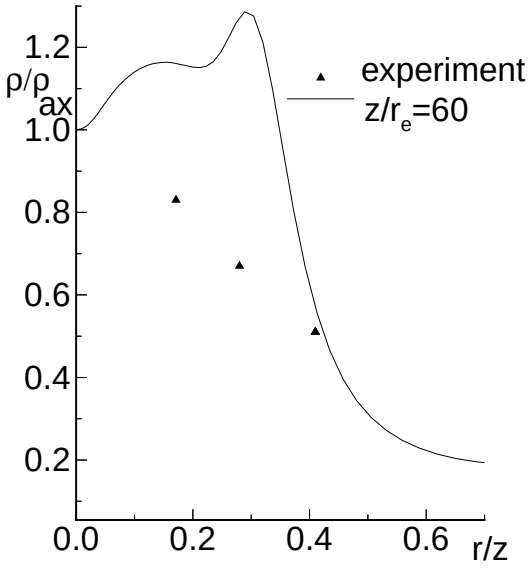

Figure 17: Transverse density profiles at $z = 60\,r_e$, ($Ma_e = 4.63$, $p_e/p_\infty = 1760.5$).

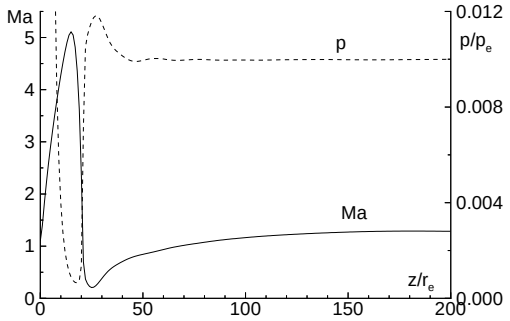

Figure 18: Distribution of pressure and Mach number along jet axis ($Ma_e = 1.1$).

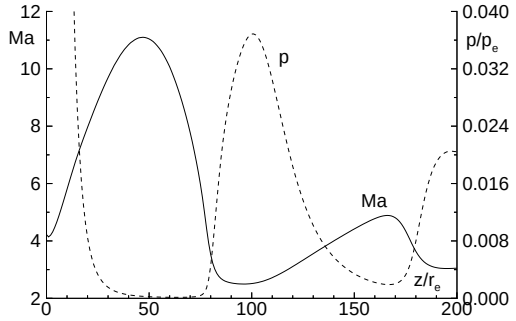

Figure 19: Distribution of pressure and Mach number along jet axis ($Ma_e = 4.22$).

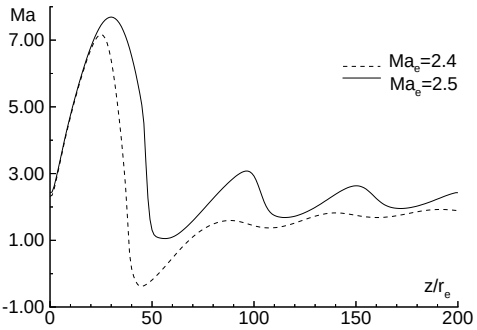

Figure 20: Regular and Mach reflection. Distribution of Mach number along jet axis. $Kn = 3.42 \times 10^{-4}$.

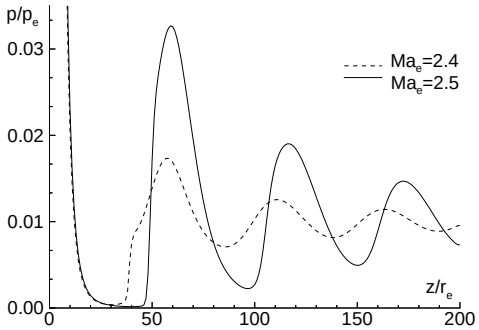

Figure 21: Regular and Mach reflection. Distribution of pressure along jet axis. $Kn = 3.42 \times 10^{-4}$.

5 Regular and Mach reflection

This set of computations was carried out to determine the range of Mach numbers where the transition between regular and Mach reflection occurs. The following parameters were retained for the jet: pressure ratio $p_\infty/p_e = 0.01$, temperature ratio $T_\infty/T_e = 1$, Knudsen number $Kn_e = 3.42 \times 10^{-4}$. As in the previous case the working gas was Nitrogen. Values of the nozzle exit Mach number were taken in the range $Ma_e = 1.1 - 4.22$. The flow at nozzle exit was taken as uniform and parallel ($\alpha_e = 0$, no boundary layer). The left boundary of the computational domain was located in the plane $z = 0$ ($l_0 = 0$). In the figures, the pressure in the jet was adimensionalized by the pressure p_e at nozzle exit.

In the case of an exit Mach number equal to 1.1, a first expansion cell is observed (Fig. 18). Along the axis the pressure decreases down to $p/p_e \approx 0.00065$ and the Mach number ($Ma = u_z/a$, where $a = \sqrt{\gamma(\mathcal{R}/\mathcal{M})T}$) reaches a maximum value approximately equal to 5. Then a Mach disk is observed. The transition from supersonic to subsonic conditions is clearly visible ($Ma \leq 1.$). The pressure increases sharply through the Mach disk, then decreases slightly to a constant value, close to the background pressure. The flow becomes isobaric and only one expansion cell is formed.

In the case of an exit Mach number equal to 4.22 the same behavior is observed in the first expansion cell, then a regular reflection takes place (Fig. 19). On the jet axis, the reflection of the barrel shock is visible as a pressure increase and a Mach number decrease. However, the Mach number remains larger than unity and the pressure exceeds the background pressure by a large factor ($\approx 4.$). A second expansion cell takes place, characterized by weaker variations of pressure and Mach number.

For intermediate Mach numbers a complex picture is observed characterized by the formation of a variable number of expansion cells (up to 4 in the computational domain for $Ma_e = 1.8$). When the Mach number increases from 1.1 to 2.4 the reflection remains a Mach reflection. For $Ma_e = 1.8 - 2.4$, a small recirculation zone (trapped vortex) forms in the subsonic zone behind the Mach disk. The same trapped vortices were observed in numerical simulations based on Navier-Stokes equations in the problem of overexpanded jet flows near the nozzle [Chen et al, (1994)] and in the problem of undererexpanded jet flows [Gribben et al. (1998)]. For $Ma_e = 2.5$ the reflection becomes regular and the subsonic zone behind the shock vanishes. Reflection remains regular up to the highest value of Ma_e investigated ($Ma_e = 4.22$).

Thus the transition from Mach to regular reflection takes place in the range of exit Mach numbers $Ma_e = 2.4 - 2.5$.The axial Mach number and pressure distributions that illustrate the transition from Mach reflection ($Ma_e = 2.4$) to regular reflection ($Ma_e = 2.5$) are shown in Figs. 20 and 21, respectively. For $Ma_e = 2.4$, the Mach number (defined as u_z/a) becomes smaller than unity, then becomes negative, which demonstrates the existence of a trapped vortex behind a Mach disk. On the contrary, for $Ma_e = 2.5$, regular reflection is observed, characterized by supersonic velocities behind the shock wave.

When Ma_e increases, the axial extent of the first expansion cell (distance along nozzle axis from nozzle exit to the first shock) also increases. At $Ma_e = 3$ only two expansion cells take place in the computational domain. The abscissa that limits the first expansion cell on the jet axis is indicated in Table 2 as estimated by Eq.1 [Abramovich (1991)] along with the corresponding values obtained from the present numerical calculations. The latter exhibit a small discontinuity when the configuration changes from Mach to regular reflection.

The comparison of the data shows that Eq. 1 gives a useful estimation whatever the type of reflection (Fig.22). The difference may be attributed to the dissipative effects that are assumed to be negligible in Eq. 1 and tend to decrease the size of the first expansion cell. The estimation given by Eqs.2 and 3 can also be used for exit Mach numbers up to approximately 2.5.

Table 2: Extent of the first expansion cell

	Mach Reflection				Regular Reflection				
Ma_e	1.1	1.8	2.2	2.4	2.5	2.6	3.0	3.4	4.22
z_{cell}/r_e	22.	30.	36.	40.	49.	52.	59.	64.	84.
$z^{AB}_{\text{cell}}/r_e(1)$	23.2	38.2	46.6	50.8	53.0	55.1	63.6	72.1	89.5
$z^{AS}_{\text{cell}}/r_e(2)$	19.6	32.1	43.8	51.2	55.4	59.8	81.2	108.9	190.8
$z^{L}_{\text{cell}}/r_e(3)$	22.4	35.9	45.9	51.6	54.6	57.7	71.1	86.3	122.9

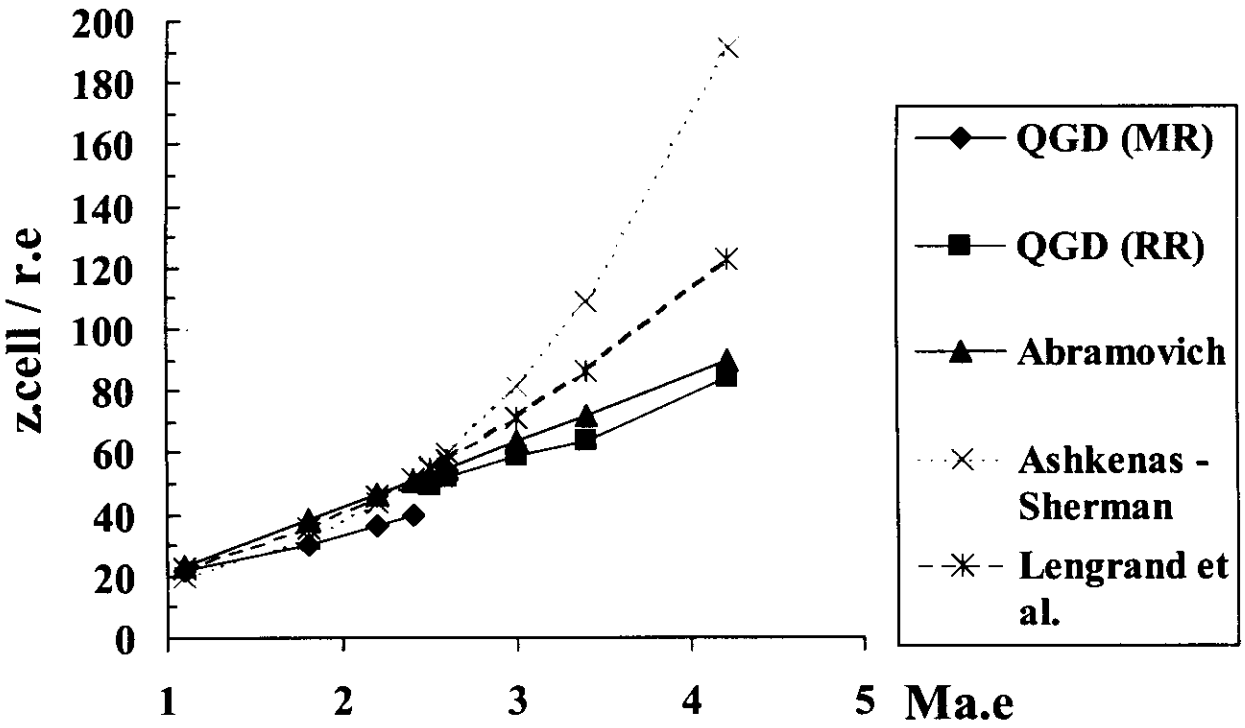

Figure 22: Extent of the first expansion cell

6 Rarefaction effects

The influence of rarefaction on the type of shock wave reflection has been investigated for a jet of monoatomic hard-sphere gas ($\omega = 0.5$, $Pr = 2/3$, $\gamma = 5/3$) with pressure ratio $p_\infty/p_e = 0.1$, temperature ratio $T_\infty/T_e = 1$ and exit Mach number $Ma_e = 1.1$. The flow was taken uniform and parallel in the nozzle exit section.

Examples of results obtained for $Kn_e = 0.002$ and 0.01 are shown as iso-Mach lines in Figs.23 and 24, respectively. Isobars have been plotted in Fig. 25 (Mach reflection) and Fig. 26 (Regular reflection). Although the shocks are rather thick, it is clear that a Mach disk is visible in Fig. 23 (Mach reflection) whereas a regular reflection (with supersonic flow behind the shock) is observed in Fig. 24. Thus an increase of Kn_e makes the configuration switch from Mach to regular reflection.

To determine when the configuration changes, the Knudsen number was varied from $Kn_e = 2 \times 10^{-4}$ to 2×10^{-2}. The resulting axial distributions of density, pressure and Mach number are plotted in Figs. 27 - 32.

For Knudsen numbers up to 2×10^{-3}, a Mach disk forms at a position that does not depend on the Knudsen number and the pressure peak behind the Mach disk decreases from 0.16 to 0.14.

For $Kn = 5 \times 10{-}3$, a regular reflection is obtained: the shock has moved somewhat downstream, the pressure peak has jumped to 0.22. However, in this special configuration the Mach number behind the reflected shock remains smaller than unity. For larger values of the Knudsen number, the regular reflection maintains, with a supersonic flow behind the shock.

Thus, it was found that the transition takes place between $Kn_e = 2 \times 10^{-3}$ and $Kn_e = 5 \times 10^{-3}$.

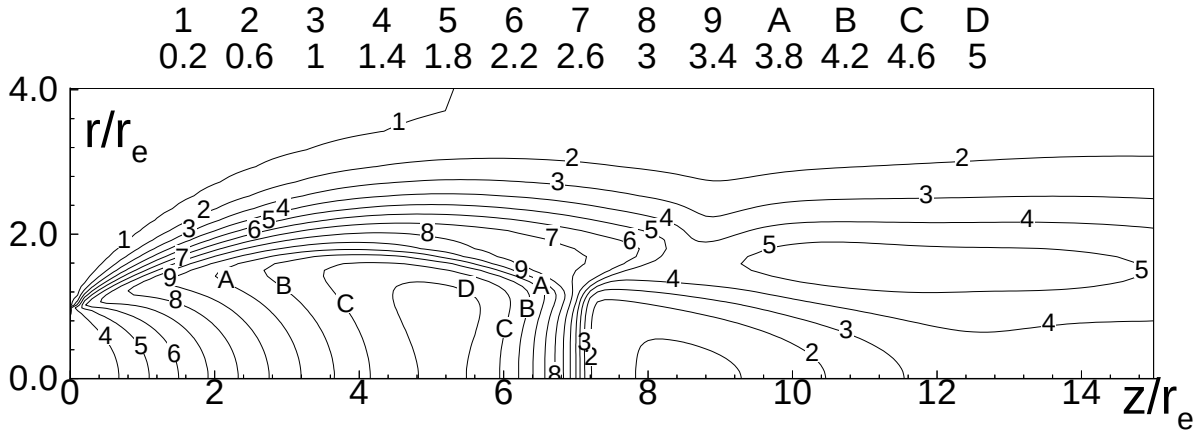

Figure 23: Iso-Mach lines. Mach reflection. $Ma_e = 1.1$, $Kn_e = 0.002$.

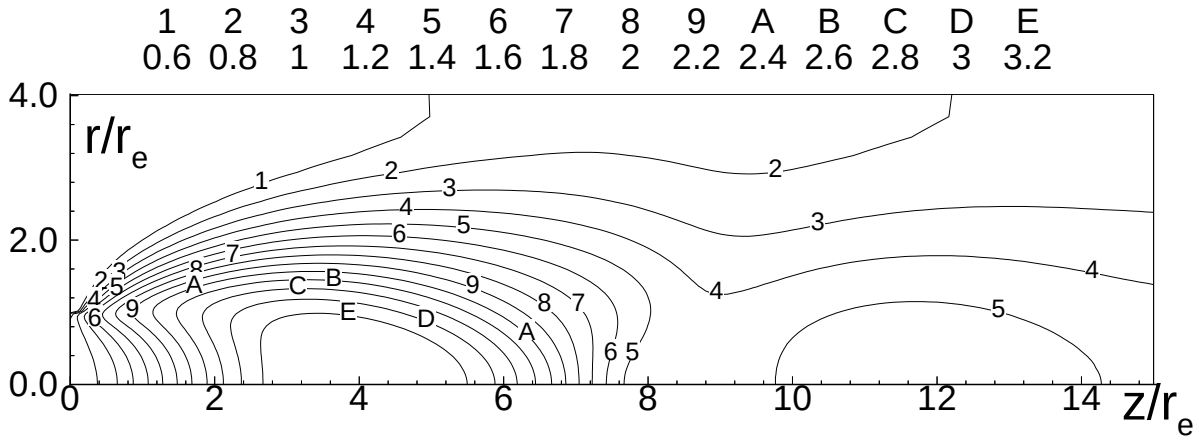

Figure 24: Iso-Mach lines. Regular reflection. $Ma_e = 1.1$, $Kn_e = 0.01$.

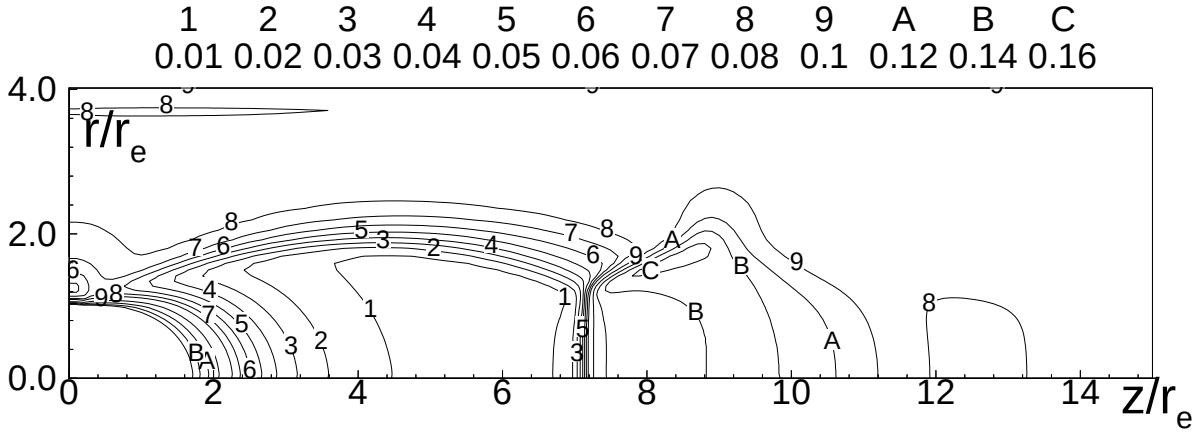

Figure 25: Isobar lines. Mach reflection. $Ma_e = 1.1$, $Kn_e = 0.002$.

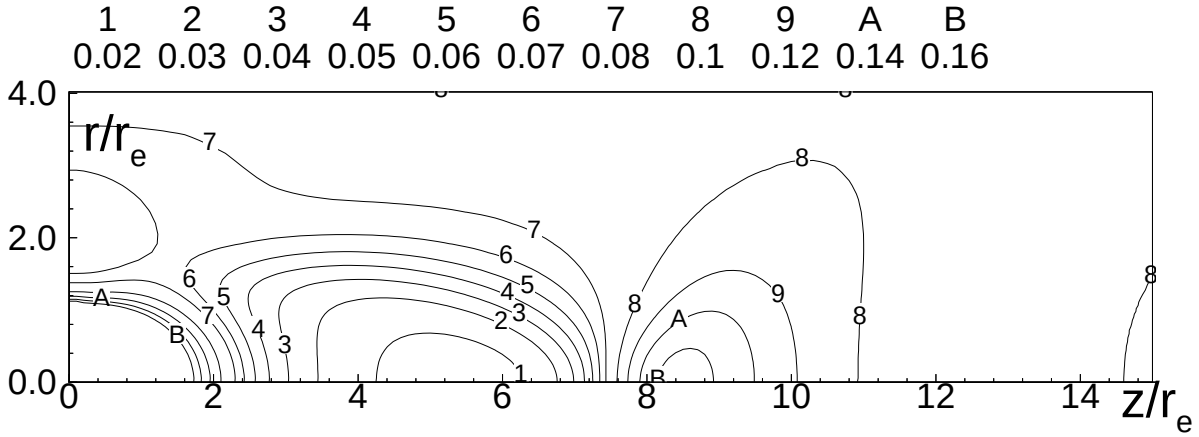

Figure 26: Isobar lines. Regular reflection. $Ma_e = 1.1$, $Kn_e = 0.01$.

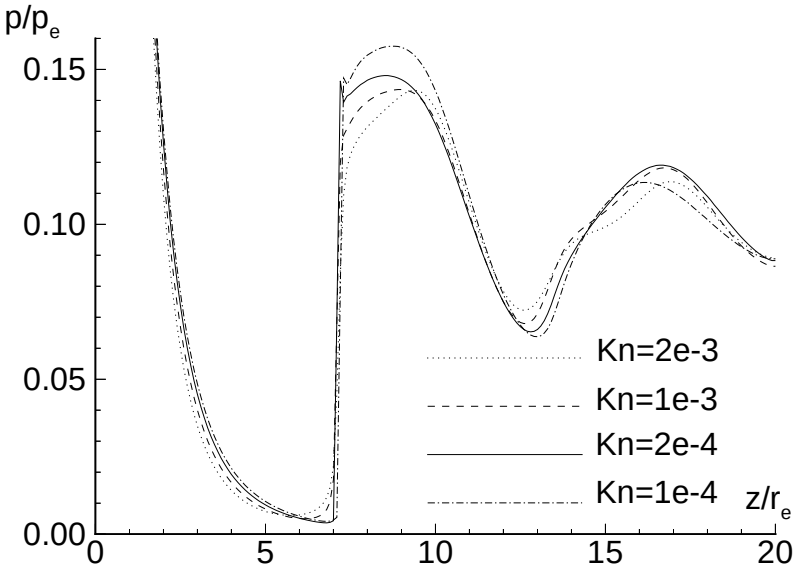

Figure 27: Mach reflection. Distribution of pressure along jet axis.

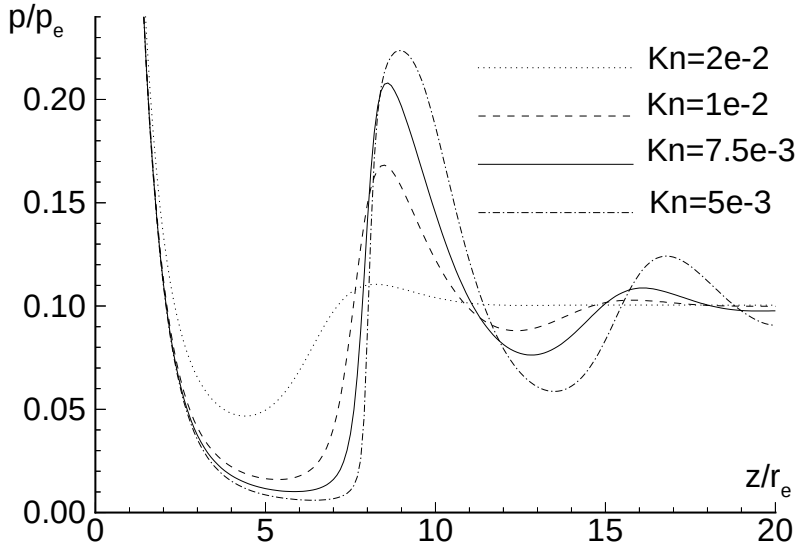

Figure 28: Regular reflection. Distribution of pressure along jet axis.

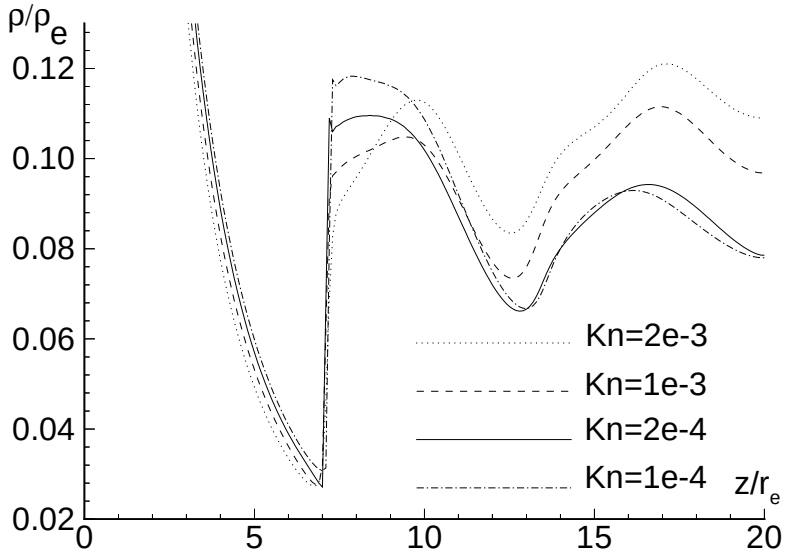

Figure 29: Mach reflection. Distribution of density along jet axis.

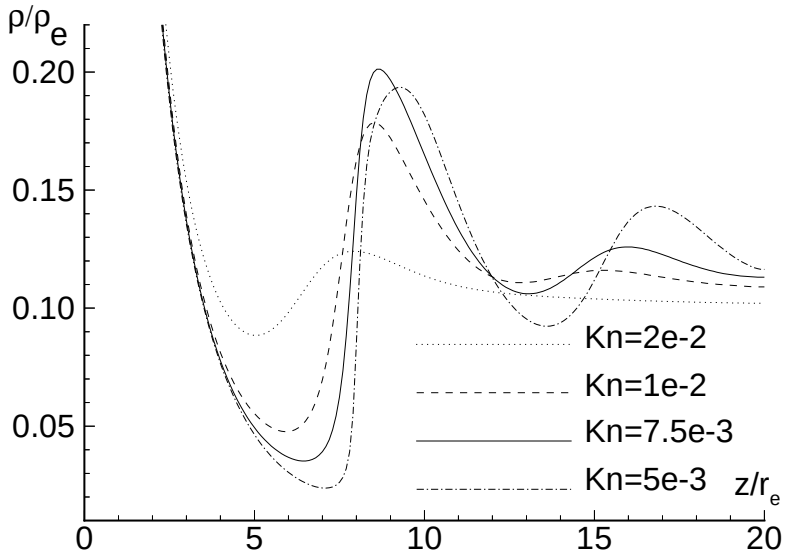

Figure 30: Regular reflection. Distribution of density along jet axis.

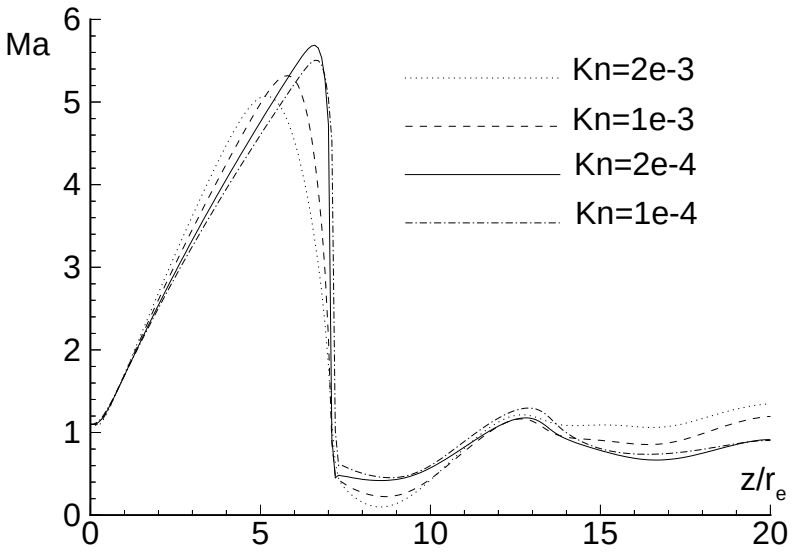

Figure 31: Mach reflection. Distribution of Mach number along jet axis.

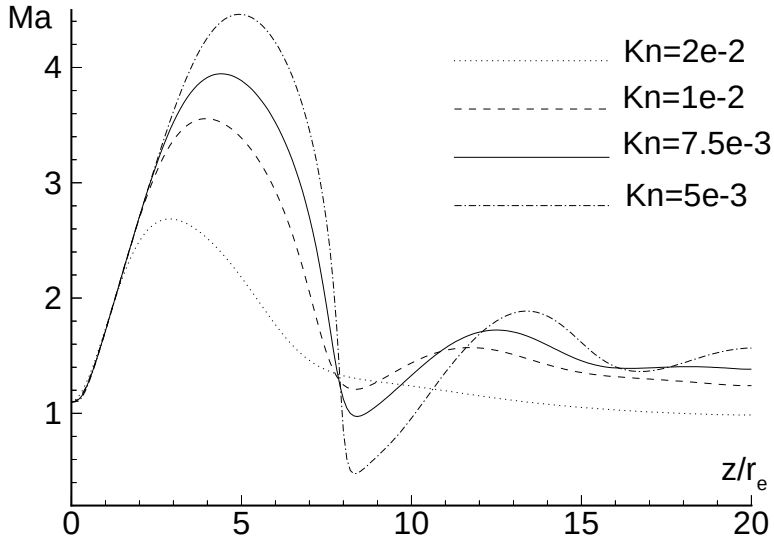

Figure 32: Regular reflection. Distribution of Mach number along jet axis.

7 Conclusion

The comparison of numerical results with experimental data and previous empirical estimations shows that the present method is an adequate tool to predict shock configurations in the underexpanded jet problem.

Transition from Mach to regular reflection has been investigated as a function of Mach and Knudsen numbers at nozzle exit.
In a Nitrogen jet with pressure ratio $p_\infty/p_e = 0.01$ transition from Mach to regular reflection takes place for exit Mach numbers in the range $Ma_e = 2.4 - 2.5$ if the Knudsen number is small ($Kn_e = 3.42 \times 10^{-4}$). Increasing Ma_e results in increasing the extent of the first expansion cell.

For a jet of hard-sphere monoatomic gas with $Ma_e = 1.1$ and $p_\infty/p_e = 0.1$, a variation of Knudsen number from 2×10^{-4} to 2×10^{-2} changes moderately the extent of the first expansion cell, but changes the reflection pattern from Mach to regular in the range $Kn_e = 2 \times 10^{-3} - 5 \times 10^{-3}$.

References

[Abramovich (1991)] Abramovich GN (1991) Applied gas dynamics. Ed. Nauka, Moscow, Vol.1 (in Russian).

[Antonov et al. (1998)] Antonov AN, Antonov MA, Graur IA, Kosarev LV, Chetverushkin BN (1998) Numerical investigations of the cavity shape on the characteristics of a pulsating gas flow, Engineering - Physical Journal, v. 71. No 3. pp. 477 – 483.

[Ashkenas (1964)] Ashkenas H and Sherman FS(1964) The structure and utilization of supersonic free jets in low density wind tunnels, Proceedings of the 4th International Symposium on Rarefied Gas Dynamics (1964), Sec. 7, Vol.2, P.84.

[Bird (1998)] Bird GA (1998) Molecular gas dynamics and the direct simulation of gas flows, Clarendon press, Oxford, 1998.

[Chen et al, (1994)] Chen CL, Chakravarthy SR, Hung CM (1994) Numerical Investigation of Separated Nozzle Flows, AIAA Journal, Vol.32, No.9, pp.1836 – 1843.

[Courant (1948)] Courant R, Friedrichs KO (1948) Supersonic flow and shock wave, Interscience Publishers, INC., New York, 1948, p.390.

[Elizarova et al. (1997)] Elizarova TG, Graur IA, Chpoun A, Lengrand JC (1997) Comparison of continuum and molecular approaches for the flow around a perpendicular disk, Proceedings of the 20th International Symposium on Shock Waves, dir. Sturtevant B. et al., World Scientific, 795–800.

[Elizarova et al. (1999)] Elizarova TG, Lengrand JC, Graur IA (1999) Gradient expansions for distribution functions and derivation of moment equations, Proceedings of 21th Intern. Symp.on RGD, Marseille, France, July 26 - 30, 1998. Ed. R.Brun. Toulouse, France, Cepadues, pp. 119 – 126.

[Gribben et al. (1998)] Gribben BJ, Cantariti F, Badcock KJ, Richards BE (1998) Numerical study of an under-expanded Jet, Proc. of the 3rd European Symp. on Aerothermodynamics for Space Vehicles, ESA SP-426:111–118.

[Lengrand et al. (1976)] Lengrand JC, Allègre J, Raffin M (1976) Experimental investigation of underexpanded exhaust plumes, AIAA J 14:692–694.

[Lengrand et al. (1982)] Lengrand JC, Allègre J, Raffin M (1982) Underexpanded free jets and their interaction with adjacent surfaces, AIAA 82-4011.

[Lengrand et al. (1995)] Lengrand JC, Chpoun A, Graur IA, Elizarova TG (1995) Supersonic rarefied gas flow around a perpendicular disk. Laboratoire d'Aérothermique du CNRS, R 95-6.

[O'Neill (1989)] O'Neill ME, Chorlton F (1989) Viscous and compressible fluid dynamics, Ellis Horwood Limited, Chichester, England, 1989.

[Sheretov (1997)] Sheretov YuV (1997) Quasihydrodynamic equations as a model for viscous compressible heat conductive flows, in book: Implementation of functional analysis in the theory of approaches, Tver University, pp.127 - 155 (in Russian).

[Shih-i Pai (1954)] Shih-i Pai (1954) Fluid dynamics of jets, D. Van Nostrand Company, INC., Canada, 1954, p. 45.

[Schlichting (1955)] Schlichting H (1955) Boundary layer theory, Pergamon press, London, 1955.